THE ASTROPHYSICAL JOURNAL, 494:285–296, 1998 February 10

DIVERSE SUPERNOVA SOURCES FOR THE *r*-PROCESS

Y.-Z. QIAN AND P. VOGEL
Department of Physics, California Institute of Technology, Pasadena, CA 91125; yzqian@citnp.caltech.edu, vogel@lamppost.caltech.edu
AND
G. J. WASSERBURG
The Lunatic Asylum, Division of Geological and Planetary Sciences, California Institute of Technology, Pasadena, CA 91125
Received 1997 June 9; accepted 1997 September 15

ABSTRACT

We present a simplified analysis using equations for the charge flow, which include ν_e capture, for the production of *r*-process nuclei in the context of the recent supernova hot bubble model. The role of ν_e capture in speeding up the charge flow, particularly at the closed neutron shells, is studied together with the β flow at freezeout and the effect of neutrino-induced neutron emission on the abundance pattern after freezeout. It is shown that a semiquantitative agreement with the gross solar *r*-process abundance pattern from the peak at mass number $A \sim 130$ through the peak at $A \sim 195$ and up to the region of the actinides can be obtained by a superposition of two distinctive kinds of *r*-process events. These correspond to a low frequency case L and a high frequency case H, which take into account the low abundance of ^{129}I and the high abundance of ^{182}Hf in the early solar nebula. The lifetime of ^{182}Hf ($\tau_{182} \approx 1.3 \times 10^7$ yr) associates the events in case H with the most common Type II supernovae. These events would be mainly responsible for the *r*-process nuclei near and above $A \sim 195$. They would also make a significant amount of the nuclei between $A \sim 130$ and 195, including ^{182}Hf, but would make very little ^{129}I. In order to match the solar *r*-process abundance pattern and to satisfy the ^{129}I and ^{182}Hf constraints, the events in case L, which would make the *r*-process nuclei near $A \sim 130$ and the bulk of those between $A \sim 130$ and 195, must occur $\sim$10 times less frequently but eject $\sim$10–20 times more *r*-process material in each event.

Assuming that all of the supernovae producing *r*-process nuclei represent a similar overall process, we speculate that the usual neutron star remnants, and hence prolonged ejection of *r*-process material, are associated with the events in case L. We further speculate that the more frequently occurring events in case H have ejection of other *r*-process material terminated by black hole formation during the neutrino cooling phase of the protoneutron star. This suggests that there is now an inventory of $\sim 5 \times 10^8$ black holes with masses $\sim 1\ M_\odot$ and $\sim 5 \times 10^7$ neutron stars resulting from supernovae in the Galaxy. This *r*-process model would have little effect on the estimates of the supernova contributions to the non–*r*-process nuclei.

Subject headings: elementary particles — nuclear reactions, nucleosynthesis, abundances — supernovae: general

1. INTRODUCTION

Approximately half of the heavy elements with mass numbers $A > 70$ and all of the actinides in the solar system are believed to have been produced in the *r*-process. The fundamental *r*-process theory of Burbidge et al. (1957) and Cameron (1957) successfully explains the gross features of the solar *r*-process abundance distribution, such as the existence of abundance peaks at $A \sim 80$, 130, and 195. On the other hand, it remains to be established where the *r*-process occurs and especially how many different kinds of *r*-process events contributed to the solar *r*-process abundances. Major advances have been made in calculating *r*-process nucleosynthesis in supernovae (see, e.g., Woosley et al. 1994) and in using a wide range of model parameters to obtain yields that approximate the solar *r*-process abundances (see, e.g., Kratz et al. 1993). There has been a tendency to ascribe all the *r*-process nuclei to a single kind of *r*-process event (cf. Goriely & Arnould 1996). However, most astrophysical models have difficulty in producing all the *r*-process abundance peaks from a single source, and the parametric studies certainly do not point to a single kind of *r*-process event.

With the recent progress in both observation and theory, there is a growing consensus that Type II supernovae are the most probable *r*-process site. The detection of *r*-process elements in the extremely metal-poor halo star CS 22892−052 by Sneden et al. (1996) argues that the *r*-process is primary, already operating in the early history of the Galaxy. Studies of Galactic chemical evolution (Mathews, Bazan, & Cowan 1992) show that the enrichment of the *r*-process elements in the Galaxy is consistent with low-mass Type II supernovae being the *r*-process sites. Furthermore, it has been proposed that the *r*-process occurs in the neutrino-heated ejecta from the hot protoneutron star produced in a Type II supernova (Woosley & Baron 1992; Woosley & Hoffman 1992; Meyer et al. 1992; Woosley et al. 1994). While this so-called "hot bubble" *r*-process model has some deficiencies, especially the need for very high entropies that might be hard to obtain (Witti, Janka, & Takahashi 1994; Takahashi, Janka, & Witti 1994; Qian & Woosley 1996; Hoffman, Woosley, & Qian 1997), it also has several attractive features. For example, the amount of ejecta from the hot bubble is consistent with the expected amount of *r*-process material from each supernova (Woosley et al. 1994), and unlike the entropy, can be understood quite well in terms of a simple neutrino-driven wind model (Qian & Woosley 1996). In addition, it has been shown that the intense neutrino flux in this kind of *r*-process

model can have important effects on nucleosynthesis (Meyer 1995; Fuller & Meyer 1995; McLaughlin & Fuller 1996, 1997; Qian et al. 1997; Haxton et al. 1997). In particular, the typical neutrino fluences through the ejecta may lead to identifiable signatures in the *r*-process abundance pattern, thus providing a way to reveal the conditions at the *r*-process site (Qian et al. 1997; Haxton et al. 1997).

Regardless of the astrophysical site, two things are needed for an *r*-process to work: the neutrons and the seed nuclei to capture them. In fact, the potential of an astrophysical environment to be the *r*-process site can be gauged by a crucial quantity, the neutron-to-seed ratio. If one always starts from more or less the same seed nuclei, different neutron-to-seed ratios are required to produce the entire solar *r*-process nuclear-abundance distribution. One can then ask whether different *r*-process nuclei are made in completely different astrophysical environments (e.g., Type II supernovae vs. neutron star coalescence) or in similar environments but just with different neutron-to-seed ratios. Because the *r*-process abundance distribution in CS 22892−052 agrees with that in the solar system quite well (Sneden et al. 1996), and the solar *r*-process abundance distribution does not have sudden jumps as a function of the mass number A, it may be more natural to expect that all *r*-process nuclei come from similar environments (e.g., the hot bubble regions in Type II supernovae). Hereafter, we refer to the production of *r*-process nuclei in a specific environment with a certain distribution of neutron-to-seed ratios as an *r*-process "event." The simplest scenario would be that all *r*-process nuclei are produced in a unique kind of *r*-process event with a generic abundance pattern. In that case, the solar *r*-process abundance distribution merely reflects the distribution of neutron-to-seed ratios characteristic of these unique *r*-process events.

However, Wasserburg, Busso, & Gallino (1996) pointed out that the above minimal approach to account for the solar *r*-process abundance distribution is not consistent with the meteoritic abundance ratios $^{129}I/^{127}I$ and $^{182}Hf/^{180}Hf$ in the early solar system. These authors showed that the *r*-process events contributing to ^{182}Hf were fully consistent with the uniform production of ^{232}Th, ^{235}U, ^{238}U, and ^{244}Pu up until the time when the solar system was formed. However, such a rather uniform production would grossly overproduce ^{129}I (by a factor of ~ 50) and ^{107}Pd (by a factor of ~ 30). Consequently, they argued that there should be diverse sources for the *r*-process, one of which produced the *r*-process nuclei above $A \sim 140$ and another producing those at lower A with a smaller frequency.

In order to account for the solar *r*-process abundance distribution and to accommodate the meteoritic data on ^{129}I and ^{182}Hf at the same time, we consider in this paper a minimal scenario where two kinds of *r*-process events contribute to the solar *r*-process abundances near and above $A \sim 130$. Using simplified treatment of the *r*-process and taking into account other constraints, we show that the main features of the solar *r*-process abundance distribution from the peak at $A \sim 130$ through the peak at $A \sim 195$ and up to the region of the actinides can be reproduced by a reasonable superposition of these two kinds of *r*-process events. Specifically, the first kind of events (case H, in which "H" stands for mainly producing the higher mass *r*-process nuclei) are mainly responsible for the *r*-process nuclei near and above $A \sim 195$. They also make a significant amount of the nuclei between $A \sim 130$ and 195, including ^{182}Hf, but very little ^{129}I. The *r*-process nuclei near $A \sim 130$ and the bulk of those between $A \sim 130$ and 195 are made in the second kind of events (case L, in which "L" stands for mainly producing the lower mass *r*-process nuclei). Furthermore, the meteoritic data on ^{129}I and ^{182}Hf allow us to associate the events in case H with the most common Type II supernovae (coincidentally, "H" also stands for occurring with a high frequency) and those in case L with the much rarer ones, which occur ~ 10 times less frequently ("L" also stands for occurring with a low frequency). In order to match the solar *r*-process abundance pattern, the rarer events in case L must eject ~ 10–20 times more *r*-process material in each event. We speculate that the events in case L leave the usual neutron star remnants and hence have prolonged ejection of *r*-process material. We further speculate that the more frequently occurring events in case H have ejection of other *r*-process material terminated by black hole formation during the neutrino cooling phase of the protoneutron star.

The organization of this paper is as follows. In § 2, we describe the hot bubble *r*-process model and our simplified *r*-process calculation in the context of this model. We also discuss the constraints on our *r*-process calculations from the observed solar *r*-process abundance distribution, the meteoritic data on ^{129}I and ^{182}Hf, and considerations of various neutrino effects. In § 3, we present our results for the two kinds of *r*-process events (cases H and L), and in § 4 we discuss their implications for the nature and frequencies of the supernovae associated with these *r*-process events.

2. SUPERNOVA *r*-PROCESS MODEL

In the following discussion, we make the general assumption that the *r*-process occurs in the neutrino-heated supernova ejecta (or in neutrino-driven winds) from the hot protoneutron star, as in the hot bubble *r*-process model. In this model, a neutron-rich mass element expands because of the heating by neutrinos emitted from the protoneutron star. The mass element initially is composed of free nucleons. As it moves away from the protoneutron star into regions of lower temperature and density, it first experiences an α particle freezeout, in which essentially all the protons are consumed, followed by an α-process (Woosley & Hoffman 1992) in which seed nuclei near $A \sim 90$ are produced. The *r*-process then takes place through the capture of the excess neutrons on these seed nuclei.

During the dynamic phase of the *r*-process, a set of progenitor nuclei are populated along the *r*-process path through neutron capture, photodisintegration, and charge-changing reactions. In the presence of an intense neutrino flux as in the hot bubble, the charge-changing reactions include ν_e capture in addition to the usual β decay. Because of the high temperature and the high neutron number density at the hot bubble *r*-process site, the neutron capture and photodisintegration reactions occur much faster than the charge-changing weak reactions. Consequently, within a given isotopic chain of charge Z, the relative abundances of the progenitor nuclei on the *r*-process path are determined by the statistical $(n, \gamma) \rightleftharpoons (\gamma, n)$ equilibrium (see, e.g., Kratz et al. 1993). The relative progenitor abundances corresponding to isotopic chains at different Z are governed by the charge-changing weak reactions. When the neutron number density drops below a critical level, the rapid neutron capture stops and the progenitor abundance pattern freezes out. The final *r*-process abundance distribu-

tion is subsequently reached through a series of charge-changing weak reactions that typically conserve the nuclear mass number A. However, β-delayed and neutrino-induced neutron emission changes A and must be included in the transformation from the neutron-rich progenitor nuclei to the observed stable r-process nuclei.

2.1. *A Simplified r-Process Calculation*

Various extensive r-process network calculations exist in the literature (see, e.g., Meyer et al. 1992; Kratz et al. 1993). However, the underlying key physics in such network calculations can be elucidated with much more modest efforts. In this paper, we adopt the following simplified r-process calculation. We start with only neutrons and seed nuclei and further assume that all seed nuclei have charge $Z_s = 34$ and mass number $A_s = 90$ typically found for the products of the α-process (Hoffman et al. 1997). We then choose an r-process path. Under the assumption of $(n, \gamma) \rightleftharpoons (\gamma, n)$ equilibrium, the r-process path approximately follows the contour of a constant neutron binding energy specified by the temperature and the neutron number density (Kratz et al. 1993). In general, this path shifts during the r-process as both the temperature and the neutron number density decrease with time. Rather than relying on the assumption of $(n, \gamma) \rightleftharpoons (\gamma, n)$ equilibrium and keeping track of the change in the r-process path, we choose an average nucleus with mass number A_Z to represent the progenitor nuclei in the isotopic chain of charge Z. In fact, the typical r-process path, especially the part at the magic neutron numbers, does not rely on the particular assumption of $(n, \gamma) \rightleftharpoons (\gamma, n)$ equilibrium. We note that for a relatively low neutron number density of $\sim 10^{20}$–10^{21} cm^{-3}, the r-process path goes through a number of common progenitor nuclei at the magic neutron numbers even if the temperature is not high enough to establish an $(n, \gamma) \rightleftharpoons (\gamma, n)$ equilibrium (Cameron et al. 1983). Thus, for simplicity, we assume in this paper that there is a fixed r-process path with a unique relation between the progenitor charge Z and the corresponding mass number A_Z. It will become clear later that this relation is used only when we evaluate the neutron-to-seed ratio corresponding to a specific abundance pattern for the progenitor nuclei at freezeout.

At the magic neutron number $N = 82$, the average nuclei on the r-process path have charges $Z = 45$–49, corresponding to $A_Z = 127$–131. Those at the magic neutron number $N = 126$ have charges $Z = 65$–69, corresponding to $A_Z = 191$–195. We use a simple linear interpolation to give A_Z for the average nuclei with nonmagic neutron numbers at $Z = 35$–44 and 50–64. Because the solar r-process abundances at $A > 209$ (e.g., the actinides) are very small, we assume that all the abundances for $A > 195$ are concentrated in an average nucleus with $A = 202$, as explained later. The chosen r-process path is shown in Figure 1. (The progenitor nuclei with magic neutron number $N = 50$ are not included in our simplified calculation because our assumed seed nuclei have neutron number $N_s > 50$. In the hot bubble r-process model, the $N = 50$ progenitor nuclei are produced in the α-process. Consequently, the solar r-process abundance peak at $A \sim 80$ usually attributed to these progenitor nuclei will not be discussed in this paper, which focuses on the r-process nuclei near and above $A \sim 130$.)

Finally, we specify the β-decay rates for these average nuclei on the r-process path. For the nuclei at the $N = 82$ and 126 closed neutron shells, we take the β-decay rates from Table 4 in Fuller & Meyer (1995) and the tabulation by Möller, Nix, & Kratz (1997). The average β-decay rates are ~ 4 and 16 s^{-1} for the progenitor nuclei with $N = 82$ and 126, respectively. Although several nuclei near $N = 82$ and $A = 130$ have experimentally measured β-decay half-lives, the β-decay properties for the majority of the progenitor nuclei have to be calculated by theory and therefore are subject to considerable uncertainties. For our simplified r-process calculation, we take an approximate β-decay rate $\lambda_\beta \approx 50$ s^{-1} for all the average nuclei with nonmagic neutron numbers (i.e., those with $Z = 34$–44 and 50–64). This rate is reasonable for the progenitor nuclei with nonmagic neutron numbers on a typical r-process path whether $(n, \gamma) \rightleftharpoons (\gamma, n)$ equilibrium is assumed or not. In fact, our conclusions do not depend sensitively on the particular choice of this rate as long as it is much larger than the β-decay rates for the progenitor nuclei with magic neutron numbers.

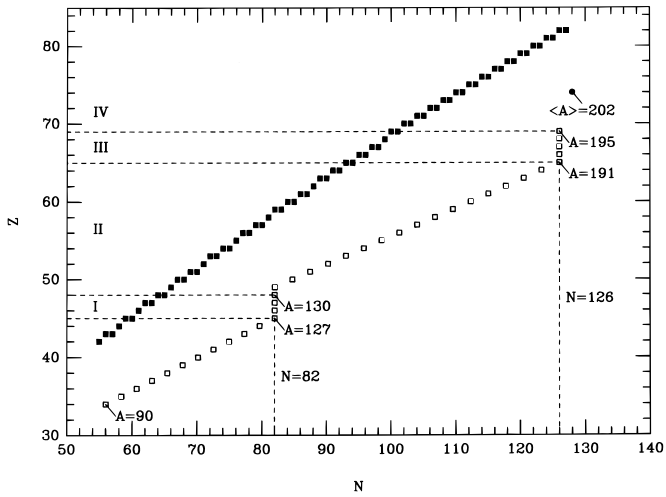

FIG. 1.—Average r-process path used in the simplified calculation. The progenitor nuclei on the path are shown as open squares on the charge (Z) vs. neutron number (N) plot. The filled squares indicate the typical nuclei at β stability. The progenitor nuclei are divided into four groups, corresponding to the four regions in the solar r-process nuclear abundance distribution: $A = 127$–130 (I), 131–190 (II), 191–195 (III), and $A > 195$ (IV). The average mass number in region IV is $\langle A \rangle = 202$. As a reminder, the magic neutron numbers are shown explicitly.

As mentioned previously, the intense neutrino flux in the hot bubble necessitates the inclusion of ν_e capture as an important type of charge-changing reaction during the supernova r-process. Furthermore, we must include ν_e capture in our r-process calculation in order to consistently study various effects of this intense neutrino flux on the r-process. The ν_e capture rates in an expanding mass element depend on the ν_e flux and, hence, on the ν_e luminosity L_{ν_e} and on the radius r of the mass element. Assuming that the ν_e luminosity evolves with time t as $L_{\nu_e}(t) = L_{\nu_e}(0) \exp(-t/\tau_\nu)$ and that the mass element expands with a constant dynamic timescale $\tau_{\rm dyn}$, i.e., $r(t) = r(0) \exp(t/\tau_{\rm dyn})$, we can write the rate for ν_e capture on an average nucleus with charge Z as

$$\lambda_{\nu_e}(Z, t) = \lambda_0(Z) \frac{L_{\nu_e, 51}(0)}{r_7(0)^2} \exp\left(-\frac{t}{\tilde{\tau}}\right), \qquad (1)$$

where $L_{\nu_e,51}$ and r_7 stand for L_{ν_e} in units of 10^{51} ergs s^{-1} and r in units of 10^7 cm, respectively, and

$$\hat{\tau} \equiv \frac{\tau_{\rm dyn}}{2} \times \frac{1}{1 + \tau_{\rm dyn}/(2\tau_\nu)} . \quad (2)$$

In equation (1), $t = 0$ is the time at which the r-process begins in the mass element expanding away from the proto-neutron star, and $\lambda_0(Z)$ is the ν_e capture rate for $L_{\nu_e} = 10^{51}$ ergs s^{-1} and $r = 10^7$ cm. We follow the calculations of Qian et al. (1997) and take $\lambda_0(Z) \approx 5.5$, 5.7, 7.0, and 8.5 s^{-1} for $Z = 34$–44, 45–49, 50–64, and 65–69, respectively.

From our previous discussion of this supernova r-process model, it follows that the abundances of progenitor nuclei on the r-process path are determined by

$$\dot{Y}(Z_s, t) = -[\lambda_\beta(Z_s) + \lambda_{\nu_e}(Z_s, t)]Y(Z_s, t) \quad (3)$$

and

$$\dot{Y}(Z, t) = [\lambda_\beta(Z-1) + \lambda_{\nu_e}(Z-1, t)]Y(Z-1, t) - [\lambda_\beta(Z) + \lambda_{\nu_e}(Z, t)]Y(Z, t) \quad (4)$$

for $Z > Z_s$. Clearly, the total abundance of all progenitor nuclei satisfy

$$\sum_{Z \geq Z_s} Y(Z, t) = Y(Z_s, 0) , \quad (5)$$

where $Y(Z_s, 0)$ is the total number of seed nuclei at the beginning of the r-process. We can define an average mass number $\bar{A}(t)$ for these progenitor nuclei through

$$\bar{A}(t)Y(Z_s, 0) = \sum_{Z \geq Z_s} A_Z\, Y(Z, t) = A_s\, Y(Z_s, t) + \sum_{Z > Z_s} A_Z\, Y(Z, t) . \quad (6)$$

From mass conservation, we have

$$Y_n(t) + \bar{A}(t)Y(Z_s, 0) = Y_n(0) + A_s\, Y(Z_s, 0) , \quad (7)$$

where Y_n is the neutron abundance. When $Y_n(t)/Y(Z_s, 0)$ becomes negligible at $t = t_{\rm FO}$, the rapid neutron capture stops, and the progenitor abundance pattern freezes out. The condition for freezeout then reads

$$\bar{A}(t_{\rm FO}) = \sum_{Z \geq Z_s} A_Z \frac{Y(Z, t_{\rm FO})}{Y(Z_s, 0)} \approx A_s + \frac{n}{s} , \quad (8)$$

where $n/s = Y_n(0)/Y(Z_s, 0)$ is the neutron-to-seed ratio.

From a set of parameters $L_{\nu_e,51}(0)/r_7(0)^2$, $\hat{\tau}$, and n/s, our simplified r-process calculation described above can be carried out in a straightforward manner. The progenitor abundance pattern at freezeout is obtained by integrating equations (3) and (4) until equation (8) is satisfied. However, the motivation of this paper is to explore the diversity of supernova r-process. Therefore, instead of adopting parameters from some specific supernova model, we treat $L_{\nu_e,51}(0)/r_7(0)^2$, $\hat{\tau}$, and n/s as free parameters. Our goal is then to find the parameters that can lead to the specific freezeout progenitor abundance patterns discussed in the next subsection.

2.2. *Constraints on the r-Process Calculation*

By employing extensive network calculations in their r-process studies, previous workers have obtained detailed freezeout abundance patterns for the progenitor nuclei and followed the subsequent β decay to stability after freezeout. Thus they can compare their final r-process abundance distributions with the observed solar r-process abundance data on a nucleus-by-nucleus basis in order to derive the varying physical conditions (e.g., neutron number density, temperature, and r-process timescale) at the r-process site or sites (Kratz et al. 1993) or to demonstrate the virtues of an astrophysical model for the r-process (Woosley et al. 1994). With our simplified r-process calculation, we are not able to make such a detailed comparison. Instead, we try to relate the essential features of the observed solar r-process abundance distribution to the freezeout progenitor abundance patterns in our calculation.

First of all, we consider only the r-process nuclei with $A \geq 127$ and divide the solar r-process abundance distribution into four regions: (I) the $A \sim 130$ peak ($A = 127$–130), (II) $A = 131$–190, (III) the $A \sim 195$ peak ($A = 191$–195), and (IV) $A > 195$ (see Fig. 1). Using the solar r-process abundance data deduced by Käppeler, Beer, & Wisshak (1989), we find that the sum of abundances in each of the first three regions satisfies

$$N_{\rm I}:N_{\rm II}:N_{\rm III} \approx 3:3:1 . \quad (9)$$

The sum of abundances for $A = 196$–209 is slightly less than that for region III. Allowing for the depletion of the actinides ($A > 209$) through fission, we assume

$$N_{\rm IV} \sim N_{\rm III} . \quad (10)$$

In general, the solar r-process abundances result from a superposition of different kinds of r-process events. Since the sum of abundances in each region is not affected very much by either β-delayed or neutrino-induced neutron emission, we take, for example, $N_{\rm I} \propto \sum_i x_i\, Y_{\rm I}^i$, where x_i is a weighting parameter and $Y_{\rm I}^i$ is the sum of the progenitor abundances in region I at freezeout in the ith kind of r-process event. As only the sum of abundances in region IV is of interest, we just need to calculate $Y(Z, t)$ for $Z_s \leq Z \leq 69$ in each kind of r-process event and then obtain $\sum_{Z>69} Y(Z, t)$ and, hence, $N_{\rm IV}$ from equation (5). Using the solar r-process abundance data, we find that the average mass number for region IV is about 202. The constraints in equations (9) and (10) apply to any r-process scenario that yields the observed solar r-process abundance pattern.

The next constraint, which distinguishes our calculation from all earlier treatments, takes into account the meteoritic data on ^{129}I/^{127}I and ^{182}Hf/^{180}Hf. As stated in the introduction, Wasserburg et al. (1996) argued that the last r-process event contributing to the ^{182}Hf in the early solar system could make only very little ^{129}I. Their argument applies to both the case where the r-process nucleosynthesis was uniform over the Galactic history and the case where the ^{129}I and ^{182}Hf in the early solar system came only from the last supernova contribution to the protosolar system within $\sim 10^7$ yr of its formation. Wasserburg et al. (1996) showed that the amount of ^{182}Hf in the early solar system is consistent with a uniform production scenario, which is also good for the actinides. According to this scenario, the last r-process event responsible for the ^{129}I in the early solar system should have occurred long ($\sim 10^8$ yr) before the last injection of ^{182}Hf, which took place within $\sim 10^7$ yr of the formation of the solar system. Consequently, there must be different r-process sources for ^{129}I and ^{182}Hf. This difference is possibly related to a distinction between the $N = 82$ and 126 closed neutron shells on the r-process path.

Based on the argument of Wasserburg et al. (1996), we consider the following minimal scenario. We assume that there are two kinds of r-process events contributing to the solar r-process abundances near and above $A \sim 130$. The first kind of events (case H) are mainly responsible for the r-process nuclei near and above $A \sim 195$ (regions III and IV). They also make a significant amount of the nuclei between $A \sim 130$ and 195 (region II), including ^{182}Hf, but very little ^{129}I. The r-process nuclei near $A \sim 130$ (region I) and the bulk of those between $A \sim 130$ and 195 are made in the second kind of events (case L). In this scenario, equations (9) and (10) can be rewritten as

$$(Y_{\rm I}^{\rm H} + xY_{\rm I}^{\rm L}):(Y_{\rm II}^{\rm H} + xY_{\rm II}^{\rm L}):(Y_{\rm III}^{\rm H} + xY_{\rm III}^{\rm L}):(Y_{\rm IV}^{\rm H} + xY_{\rm IV}^{\rm L}) \approx 3:3:1:1 , \quad (11)$$

where for example, $Y_{\rm I}^{\rm H}$ is the sum of progenitor abundances (normalized according to eq. [5]) in region I in case H, and x is a weighting parameter to be determined by our calculation. Physically, the weighting parameter x depends on the amount of r-process material produced in a single event and the frequency of such events in both cases H and L. Note that the quantities on the left-hand side of equation (11), e.g., $Y_{\rm I}^{\rm H} + xY_{\rm I}^{\rm L}$, are proportional to the sums of solar r-process abundances in the corresponding regions, e.g., $N_{\rm I}$, in equations (9) and (10).

Ideally, we would like to have no production of ^{129}I at all in case H. Practically, we can set an upper limit on the ^{129}I production in case H as follows. We assume that all the ^{129}I in the early solar system was produced by the r-process events in case H. This could be realized if the period between the last r-process event in case L and the formation of the solar system was long ($\sim 10^8$ yr) compared with the lifetime of ^{129}I ($\tau_{129} \approx 2.3 \times 10^7$ yr). We assume that this is the case in the following discussion. Meteoritic measurements give the abundance ratio $^{129}{\rm I}/^{127}{\rm I} \approx 10^{-4}$ in the early solar system, which corresponds to $^{129}{\rm I}/^{195}{\rm Pt} \approx 1.9 \times 10^{-4}$. In the uniform production scenario, the abundance ratio $^{129}{\rm I}/^{195}{\rm Pt}$ in the early solar system is

$$\frac{^{129}{\rm I}}{^{195}{\rm Pt}} \approx \frac{Y^{\rm H}(Z = 47, t_{\rm FO})}{Y^{\rm H}(Z = 69, t_{\rm FO})} \frac{\tau_{129}}{t_G} , \quad (12)$$

where $Y^{\rm H}(Z, t_{\rm FO})$ stands for $Y(Z, t_{\rm FO})$ in case H, and $t_G \approx 10^{10}$ yr is the period of Galactic r-process nucleosynthesis prior to the formation of the solar system. The upper limit on the production of ^{129}I in case H is then

$$\frac{Y^{\rm H}(Z = 47, t_{\rm FO})}{Y^{\rm H}(Z = 69, t_{\rm FO})} \sim 0.1 . \quad (13)$$

In deriving the above upper limit, we have assumed that the final abundances of ^{129}I and ^{195}Pt are approximately the same as the progenitor abundances for $(Z, A) = (47, 129)$ and (69, 195) in case H. This assumption is reasonable because the β-delayed neutron emission probabilities of the progenitor nuclei at and immediately above $A = 129$ and 195 are small, and neutrino-induced neutron emission after freezeout is severely constrained as discussed below.

Furthermore, it is believed that the abundance peaks at $A \sim 130$ and 195 owe their existence to the slow β-decay rates of the progenitor nuclei at the $N = 82$ and 126 closed neutron shells. In fact, Kratz et al. (1988) showed that the product of the freezeout progenitor abundance at the closed neutron shells and the corresponding β-decay rate is approximately constant; i.e., a steady-state β-flow equilibrium approximately holds for these progenitor nuclei at freezeout. Accordingly, we adopt the constraint

$$\frac{\lambda_\beta(Z)Y(Z, t_{\rm FO})}{\lambda_\beta(Z + 1)Y(Z + 1, t_{\rm FO})} \approx 1 \pm 0.2 \quad (14)$$

for $Z = 45$–47 (case L) and 65–68 (case H) in our r-process calculation. As pointed out by Fuller & Meyer (1995), the constraint in equation (14) is especially important when ν_e capture is included in the r-process calculation. It requires that β decay be the dominant charge-changing reaction when the abundance peaks freeze out; i.e., it restricts the ν_e flux at $t = t_{\rm FO}$.

Finally, we consider the effects of neutrino-induced neutron emission after freezeout. Qian et al. (1997) and Haxton et al. (1997) showed that neutrino-induced neutron emission results in significant production of the nuclei in the valleys immediately below the abundance peaks even for moderate neutrino fluences after freezeout. In order to produce the right amount of these nuclei, the neutrino fluence $\mathcal{F}$ after freezeout has to be sufficiently low. For case H, we have

$$\mathcal{F} = \frac{L_{\nu_e,51}(0)}{r_7(0)^2} \exp\left(-\frac{t_{\rm FO}}{\hat{\tau}}\right)\hat{\tau} \approx 0.015 , \quad (15)$$

and for case L

$$\mathcal{F} = \frac{L_{\nu_e,51}(0)}{r_7(0)^2} \exp\left(-\frac{t_{\rm FO}}{\hat{\tau}}\right)\hat{\tau} \approx 0.031 . \quad (16)$$

(The upper limits on $\mathcal{F}$ are 0.030 in case H and 0.045 in case L in order not to overproduce these nuclei in the valleys.)

The constraints in equations (9)–(11) are treated in more accurate forms in earlier r-process network calculations, but those in equations (13), (15), and (16) have not been considered. While equation (14) is found to hold in earlier r-process calculations (see, e.g., Kratz et al. 1993), its validity is essentially guaranteed by the constraints in equations (15) and (16) in our calculation. In the future, full network calculations will have to be carried out in order to include the ^{129}I and ^{182}Hf data and to allow for various neutrino effects. In this regard, our simplified r-process calculation serves as an illustration of the spirit and, hopefully, as a stimulus for more sophisticated future studies.

3. RESULTS AND DISCUSSION

As stated earlier, there are three parameters, $L_{\nu_e,51}(0)/r_7(0)^2$, $\hat{\tau}$, and n/s, in our simplified r-process calculation. Before we present the results of our calculation, it is helpful to discuss the physics that relates the set of these three parameters to the progenitor abundance pattern at freezeout in case H or L. Obviously, in both cases the neutron-to-seed ratio n/s is related to the average progenitor mass number $\bar{A}(t_{\rm FO})$ at freezeout through equation (8). The mass number A_Z of a progenitor nucleus is approximately proportional to its charge Z; i.e., $A_Z \approx kZ$, where the proportionality constant is $k \approx 2.6$–2.9 for the r-process path shown in Figure 1. Therefore, the average progenitor charge $\bar{Z}(t_{\rm FO})$ at freezeout is

$$\bar{Z}(t_{\rm FO}) = \sum_{Z \geq Z_s} Z \frac{Y(Z, t_{\rm FO})}{Y(Z_s, 0)} \approx \frac{\bar{A}(t_{\rm FO})}{k} . \quad (17)$$

From equations (8) and (17) we obtain

$$\frac{n}{s} \approx k\bar{Z}(t_{\rm FO}) - A_s \,, \tag{18}$$

and we assume $k \approx 2.7$ in the following discussion.

Because only charge-changing reactions are involved in equations (3) and (4), we can approximately view the r-process as a charge flow proceeding from Z_s to successively higher Z, accompanied by the capture of $A_Z - A_s$ neutrons at each Z. When the neutrons run out at $t = t_{\rm FO}$, the charges in the flow have an average value $\bar{Z}(t_{\rm FO})$. Without solving equations (3) and (4) for the charge flow, we can approximately calculate this average progenitor charge $\bar{Z}(t_{\rm FO})$ at freezeout as

$$\bar{Z}(t_{\rm FO}) = Z_s + \bar{\lambda}_\beta t_{\rm FO} + \bar{\lambda}_{\nu_e}(0)\hat{\tau}\left[1 - \exp\left(-\frac{t_{\rm FO}}{\hat{\tau}}\right)\right], \tag{19}$$

where $\bar{\lambda}_\beta$ is the average β-decay rate and $\bar{\lambda}_{\nu_e}(0)$ is the average initial ν_e capture rate [proportional to $L_{\nu_e,51}(0)/r_7(0)^2$], both appropriately taken for the progenitor nuclei involved in the calculation. Equation (19) then relates $L_{\nu_e,51}(0)/r_7(0)^2$, $\hat{\tau}$, and the freezeout time $t_{\rm FO}$ to the progenitor abundance pattern at freezeout in both cases H and L.

Furthermore, $L_{\nu_e,51}(0)/r_7(0)^2$, $\hat{\tau}$, and $t_{\rm FO}$ are subject to the neutrino fluence constraints in equations (15) and (16) for cases H and L, respectively. Therefore, one can use either $L_{\nu_e,51}(0)/r_7(0)^2$ or $\hat{\tau}$ as the only adjustable parameter in the two cases. Once chosen, the other parameter, together with the freezeout time $t_{\rm FO}$, is determined by the average progenitor charge at freezeout (eq. [19]) and the neutrino fluence constraint (eq. [15] or [16]) in each case.

3.1. *Results for a Given* $L_{\nu_e,51}(0)/r_7(0)^2$

For the convenience of presentation, we first give results for a reasonable value of $L_{\nu_e,51}(0)/r_7(0)^2 \approx 8.77$, which corresponds to $\lambda_{\nu_e}(Z, 0) \approx 50\ {\rm s}^{-1}$ for the progenitor nuclei with $N = 82$. The dependence of our results on $L_{\nu_e,51}(0)/r_7(0)^2$ will be examined in § 3.3. Our best fit for case H is obtained for $\hat{\tau} \approx 0.186$ s and $n/s \approx 92$. The corresponding freezeout time is $t_{\rm FO} \approx 0.86$ s. The time evolution of the progenitor abundance pattern in case H is shown in Figure 2 as a series of snapshots. Similarly, the best fit for case L is obtained for $\hat{\tau} \approx 0.125$ s and $n/s \approx 48$, with the corresponding freezeout time $t_{\rm FO} \approx 0.44$ s. The time evolution of the progenitor abundance pattern in case L is shown in Figure 3. For a given $L_{\nu_e,51}(0)/r_7(0)^2$, we find that case H is specified essentially by the constraint on ^{129}I production in equation (13) and the neutrino fluence constraint in equation (15). With the freezeout pattern obtained in case H, case L is specified by the solar r-process abundance ratios in equation (11) and the neutrino fluence constraint in equation (16). The weighting parameter in equation (11) is found to be $x \approx 2.17$. With the above best-fit parameters, all the constraints discussed in § 2.2 are satisfied.

The abundance pattern obtained from the superposition of cases H and L is shown in Figure 4. As explained previously, we cannot compare this pattern with the solar r-process abundance distribution on a nucleus-by-nucleus basis, especially because we do not follow the transform-

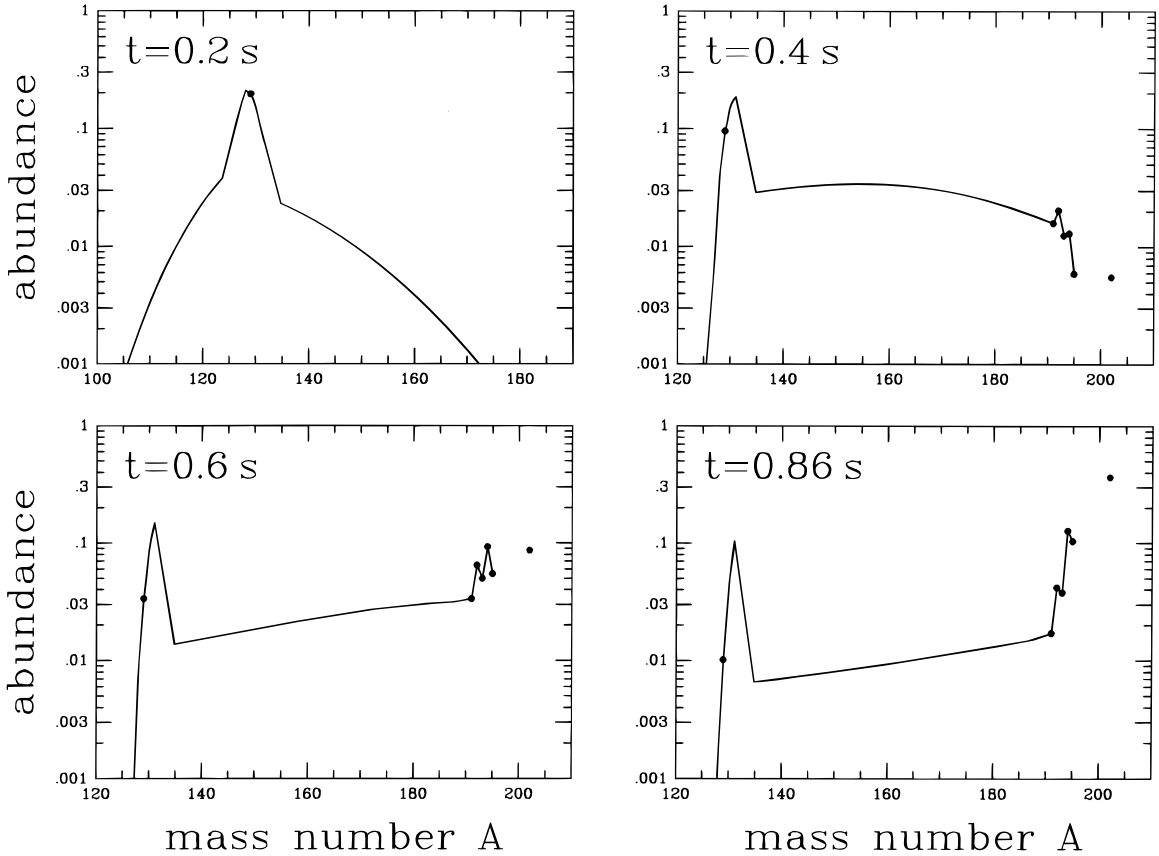

FIG. 2.—Time evolution of the progenitor abundance pattern in case H, assuming $L_{\nu_e,51}/r_7(0)^2 \approx 8.77$, $\hat{\tau} \approx 0.186$ s, and $n/s \approx 92$. The sum of all progenitor abundances is normalized to unity. The progenitor abundances at $A = 129$ and 191–195 are shown as filled circles. The sum of progenitor abundances at $A > 195$ is indicated as the filled circle at $A = 202$. The progenitor abundance pattern freezes out at $t = t_{\rm FO} \approx 0.86$ s and satisfies all the constraints discussed in § 2.2.

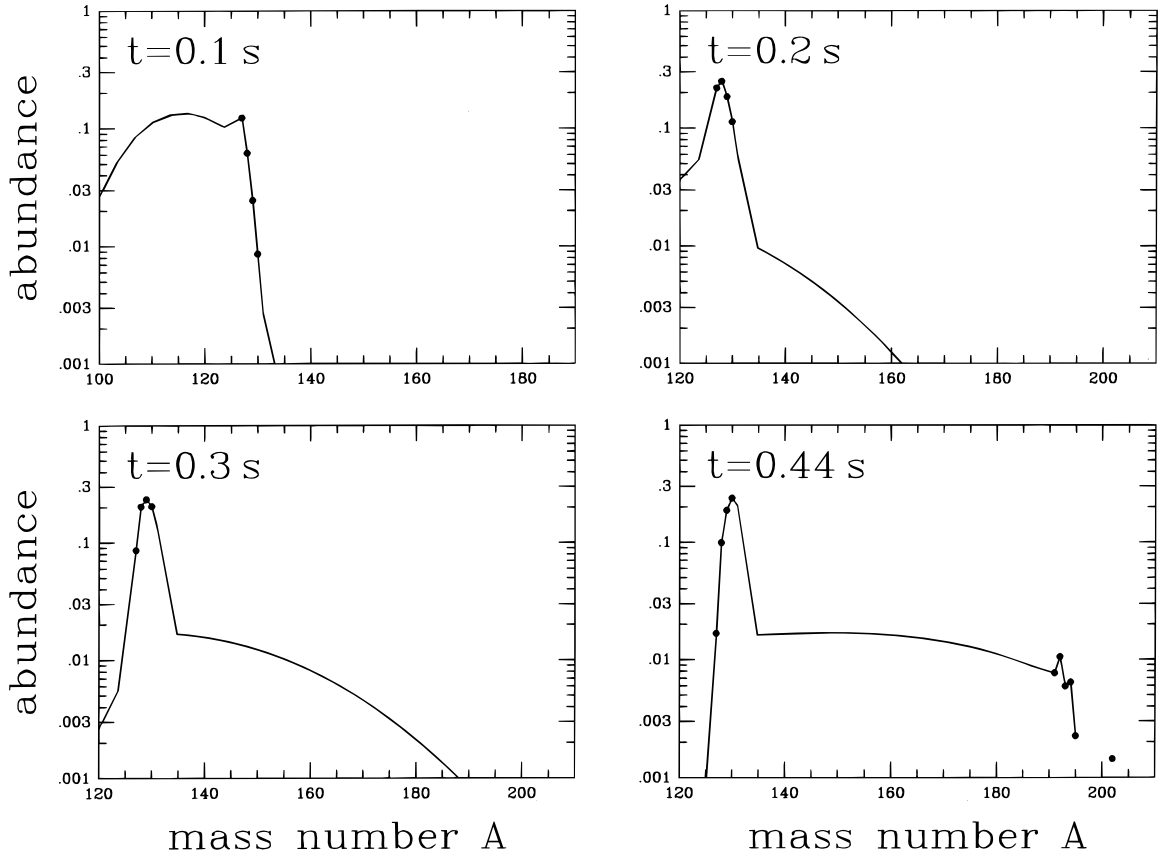

FIG. 3.—Time evolution of the progenitor abundance pattern in case L, assuming $L_{\nu_e,51}/r_7(0)^2 \approx 8.77$, $\hat{\tau} \approx 0.125$ s, and $n/s \approx 48$. The sum of all progenitor abundances is normalized to unity. The progenitor abundances at $A = 127$–130 and 191–195 are shown as filled circles. The sum of progenitor abundances at $A > 195$ is indicated as the filled circle at $A = 202$. The progenitor abundance pattern freezes out at $t = t_{FO} \approx 0.44$ s and satisfies all the constraints discussed in § 2.2.

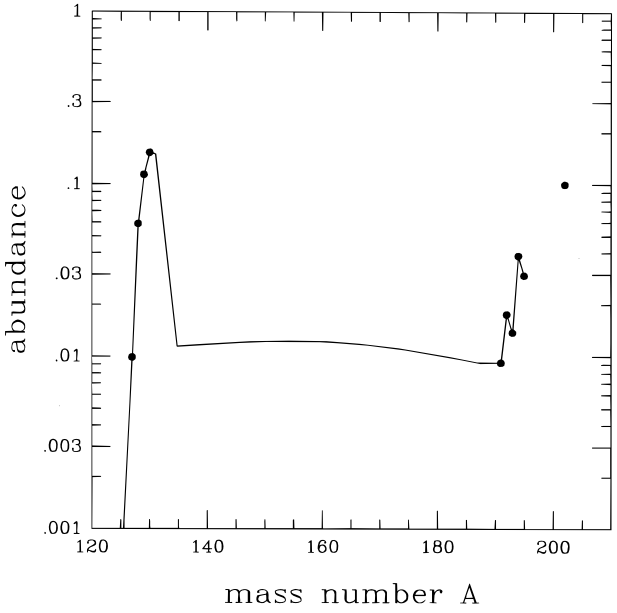

FIG. 4.—Abundance pattern that matches the bulk solar r-process abundances in regions I, II, III, and IV for the minimal two-component model (see text). This pattern is obtained by superposing the freezeout progenitor abundance pattern in case H with that in case L. The freezeout progenitor abundance pattern in case L is weighted by a factor of 2.17 with respect to that in case H. The abundances at $A = 127$–130 and 191–195 are shown as filled circles. The sum of abundances at $A > 195$, indicated as the filled circle at $A = 202$, is chosen to be 0.1. All the other abundances are scaled accordingly.

ation from the progenitor nuclei to the stable r-process nuclei after freezeout. However, if we assume that the progenitor nuclei at the $N = 82$ and 126 closed neutron shells approximately conserve their mass numbers during the transformation after freezeout, the final abundances at these mass numbers (regions I and III) shown in Figure 4 agree with the solar r-process abundances in the $A \sim 130$ and 195 peaks quite well. While we cannot obtain detailed abundances for the r-process nuclei in regions II and IV mainly because of significant β-delayed neutron emission expected in these two regions after freezeout, at least the sums of the abundances in these two regions, together with those in regions I and III, agree with the solar r-process abundance pattern as required by our calculation.

Furthermore, we can show that the abundance ratio $^{182}Hf/^{180}Hf$ in the early solar system is also consistent with the meteoritic data and with the scenario where the r-process events in both cases H and L occurred uniformly up until the formation of the solar system. As explained previously, the constraint on ^{129}I production requires that the last r-process event in case L contributing to the solar abundances occur $\sim 10^8$ yr before the formation of the solar system. Because the lifetime of ^{182}Hf is $\tau_{182} \approx 1.3 \times 10^7$ yr $\ll 10^8$ yr, the ^{182}Hf made in this last r-process event in case L had already decayed to the stable ^{182}W when the solar system was formed. Following Wasserburg et al. (1996), we take $^{182}W_r/^{180}Hf \approx 0.37$, where $^{182}W_r$ represents the r-process contribution to the solar abundance of ^{182}W.

In the uniform production scenario, we have

$$\frac{^{182}\mathrm{Hf}}{^{182}\mathrm{W}_r} \approx \frac{Y^{\mathrm{H}}_{182}}{Y^{\mathrm{H}}_{182} + xY^{\mathrm{L}}_{182}} \times \frac{\tau_{182}}{t_G}, \quad (20)$$

where Y^{H}_{182} and Y^{L}_{182} stand for the final abundances of ^{182}Hf in cases H and L, respectively. Assuming $Y^{\mathrm{H}}_{182} \sim Y^{\mathrm{L}}_{182}$ (cf. Figs. 2 and 3), we obtain $^{182}\mathrm{Hf}/^{182}\mathrm{W}_r \sim 4.1 \times 10^{-4}$, which corresponds to $^{182}\mathrm{Hf}/^{180}\mathrm{Hf} \sim 1.5 \times 10^{-4}$, which is in good agreement with the meteoritic value $^{182}\mathrm{Hf}/^{180}\mathrm{Hf} \approx 2.8 \times 10^{-4}$. In fact, we can always obtain this agreement as long as $Y^{\mathrm{H}}_{182} \gtrsim Y^{\mathrm{L}}_{182}$ and $x \sim 1$.

We now examine the effect of ν_e capture on the charge flow. In our calculation, equations (15) and (16), which concern the neutrino fluence after freezeout, impose much more stringent constraints on the ν_e flux than does equation (14), which concerns the approximate β-flow equilibrium at freezeout. This result was found earlier by Qian et al. (1997). By the time the progenitor abundance pattern freezes out, the charge flow is carried dominantly by β decay in both cases H and L. However, whereas equation (14) is satisfied for all five progenitor nuclei ($Z = 65$–69) in the $N = 126$ peak in case H, it is satisfied for only three progenitor nuclei ($Z = 46$–48) in the $N = 82$ peak in case L. This is because the bottleneck in the charge flow caused by the slow β-decay rates for the $N = 82$ progenitor nuclei facilitates the establishment of an approximate β-flow equilibrium in the $N = 126$ peak in case H, whereas no corresponding bottleneck exists before the $N = 82$ progenitor nuclei in case L. On the other hand, ν_e capture accelerates the charge flow quite noticeably in both cases H and L.

We recall that for given values of $L_{\nu_e,51}(0)/r_7(0)^2$ and $\hat{\tau}$, equation (19) determines the freezeout time t_{FO} as a function of the average progenitor charge $\bar{Z}(t_{\mathrm{FO}})$ at freezeout. Here we give a more accurate way to evaluate this function. The time $\delta t(Z)$ required for the charge flow to pass through the progenitor nucleus at charge Z is approximately determined by

$$\lambda_\beta(Z_s)\delta t(Z_s) + \lambda_{\nu_e}(Z_s, 0)\hat{\tau}\left\{1 - \exp\left[-\frac{\delta t(Z_s)}{\hat{\tau}}\right]\right\} \approx 1 \quad (21)$$

and

$$\lambda_\beta(Z)\delta t(Z) + \lambda_{\nu_e}[Z, t(Z)]\hat{\tau}\left\{1 - \exp\left[-\frac{\delta t(Z)}{\hat{\tau}}\right]\right\} \approx 1 \quad (22)$$

for $Z > Z_s$, where $t(Z) = \sum_{Z'=Z_s}^{Z-1} \delta t(Z')$ is the time required for the charge flow to proceed from Z_s up to Z. We assume that the freezeout time t_{FO} is approximately given by

$$t_{\mathrm{FO}} = t[\bar{Z}(t_{\mathrm{FO}})] \approx \sum_{Z=Z_s}^{\bar{Z}(t_{\mathrm{FO}})-1} \delta t(Z), \quad (23)$$

with $t_{\mathrm{FO}} = 0$ for $\bar{Z}(t_{\mathrm{FO}}) = Z_s$. It is easy to see that equation (19) is obtained by replacing $\lambda_\beta(Z)$ and $\lambda_{\nu_e}(Z, 0)$ for $Z \geq Z_s$ with $\bar{\lambda}_\beta$ and $\bar{\lambda}_{\nu_e}(0)$ in equations (21) and (22). Using equations (21)–(23), we plot t_{FO} as a function of the average progenitor charge $\bar{Z}(t_{\mathrm{FO}})$ at freezeout for $L_{\nu_e,51}(0)/r_7(0)^2 \approx 8.77$ and $\hat{\tau} \approx 0.186$ and 0.125 s, and for the case without neutrinos in Figure 5. The time required to reach the same average progenitor charge at freezeout is clearly longer without neutrinos than with neutrinos. The actual freezeout times t_{FO} in cases H and L are indicated as filled circles in Figure 5. The shortening of t_{FO} in both cases with respect to the case without neutrinos (see § 3.2) mainly results from the ν_e capture–induced acceleration of the charge flow at $Z = 45$–49, i.e., at the progenitor nuclei with the $N = 82$ closed neutron shell.

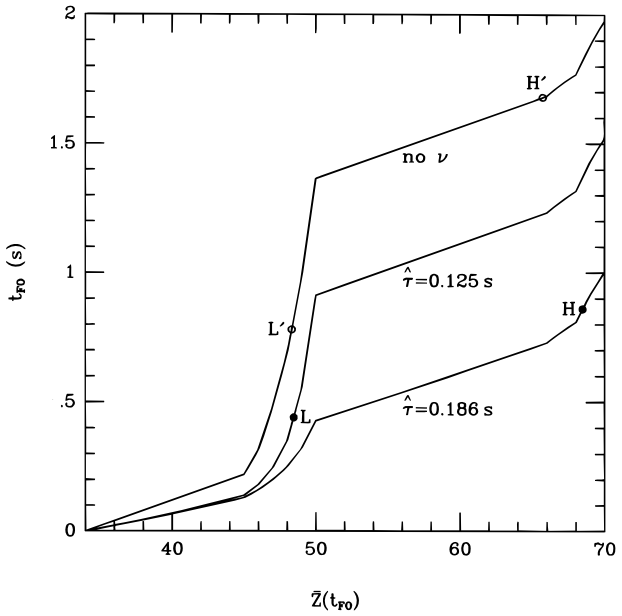

FIG. 5.—Freezeout time t_{FO} as a function of the average progenitor charge $\bar{Z}(t_{\mathrm{FO}})$ at freezeout for $L_{\nu_e,51}/r_7(0)^2 \approx 8.77$, $\hat{\tau} \approx 0.186$ and 0.125 s, and for the case without neutrinos. The actual freezeout time $t_{\mathrm{FO}} \approx 0.86$ (0.44) s in case H (L) is indicated as the filled circle labelled H (L). Note that approximately the same average progenitor charge at freezeout as in case H (L) is reached at a considerably longer freezeout time $t_{\mathrm{FO}} \approx 1.68$ (0.78) s in the case without neutrinos [the open circle labelled H′ (L′)].

To conclude this subsection, we give a semianalytic way to derive $\hat{\tau}$ and n/s in cases H and L for a given $L_{\nu_e,51}(0)/r_7(0)^2$. As discussed in the beginning of § 3, the neutron-to-seed ratio n/s is approximately given by the average progenitor charge $\bar{Z}(t_{\mathrm{FO}})$ at freezeout via equation (18). From the solar r-process abundance ratios in equation (11) and the constraint on ^{129}I production in equation (13), we see that a large fraction of the progenitor abundances should be in region III (I) at freezeout in case H (L). Consequently, the average progenitor charge at freezeout has to be $\bar{Z}(t_{\mathrm{FO}}) \approx 68$–$69$ (48–49) in case H (L), which requires a neutron-to-seed ratio of $n/s \approx 94$–96 (40–42) in good agreement with our numerical results. Once $\bar{Z}(t_{\mathrm{FO}})$ is known, the freezeout time t_{FO} can be calculated as a function of $\hat{\tau}$ for a given $L_{\nu_e,51}(0)/r_7(0)^2$ using equations (21)–(23). The contours for $\bar{Z}(t_{\mathrm{FO}}) = 48$, 49, 68, and 69 are shown as solid lines on the $\hat{\tau}$-t_{FO} plot in Figure 6. Furthermore, the neutrino fluence constraint in equation (15) or (16) gives t_{FO} as another function of $\hat{\tau}$ for a given $L_{\nu_e,51}(0)/r_7(0)^2$. The contours for values of the neutrino fluence after freezeout $\mathscr{F} = 0.015$ and 0.031 are shown as dashed lines in Figure 6. The best-fit parameters for t_{FO} and $\hat{\tau}$ in case H (L) should then lie on the dashed line for $\mathscr{F} = 0.015$ (0.031) and between the solid lines for $\bar{Z}(t_{\mathrm{FO}}) = 68$ (48) and 69 (49). This is confirmed by our numerical results, which are indicated as filled circles in Figure 6.

3.2. *Results for the Case without Neutrinos*

We now consider the case without neutrinos, i.e., $L_{\nu_e,51}(0)/r_7(0)^2 = 0$. Obviously, the neutrino fluence constraints in equations (15) and (16) can no longer be satisfied and can be treated only as some upper limits on the neu-

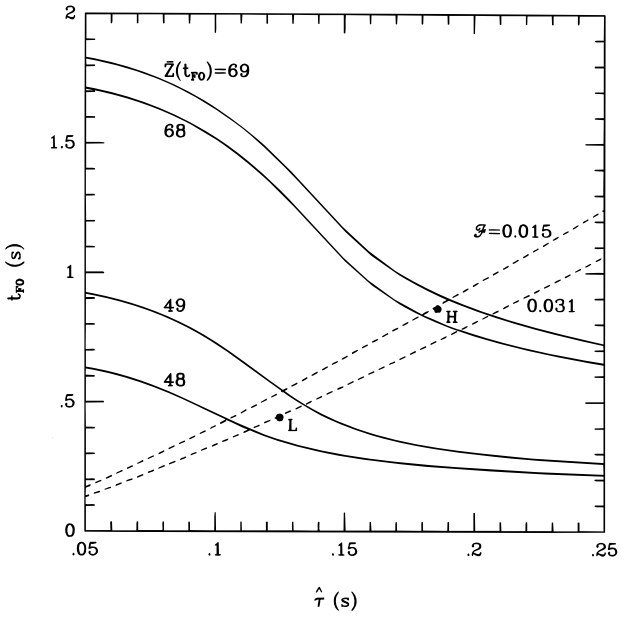

FIG. 6.—Determination of $\hat{\tau}$ and t_{FO} in cases H and L for $L_{\nu_e,51}/r_7(0)^2 \approx 8.77$. The solid lines give the contours for values of the average progenitor charge at freezeout $\bar{Z}(t_{FO}) = 48$, 49, 68, and 69, as calculated from eqs. (21), (22), and (23), on the $\hat{\tau}$-t_{FO} plot. The dashed lines give the contours for values of the neutrino fluence after freezeout $\mathcal{F} = 0.015$ and 0.031, as calculated from eqs. (15) and (16), on the same plot. The filled circles labelled H and L indicate the best-fit parameters in cases H and L, respectively, which satisfy the corresponding equations for $\bar{Z}(t_{FO})$ and $\mathcal{F}$.

trino fluence after freezeout in this case. By leaving out neutrinos and the associated constraints in equations (15) and (16), we also find freezeout progenitor abundance patterns that can satisfy essentially all the other constraints discussed in § 2.2. These freezeout progenitor abundance patterns corresponding to cases H′ and L′ are similar to those in cases H and L presented in § 3.1 but are obtained with slightly smaller neutron-to-seed ratios and considerably longer freezeout times. The neutron-to-seed ratio in case H′ (L′) is $n/s \approx 86$ (44) with the corresponding freezeout time $t_{FO} \approx 1.68$ (0.78) s. As shown in Figure 5, approximately the same average progenitor charge at freezeout is reached in cases H and H′ or in cases L and L′. The weighting parameter in equation (11) is $x \approx 1.11$ for case L′ with respect to case H′ in order to give the best fit to the gross solar r-process abundance pattern. The time evolution of the progenitor abundance pattern in the case without neutrinos is shown in Figure 7.

Here we notice some interesting differences between cases H′ (L′) and H (L). Case H′ is essentially determined by the constraint on ^{129}I production in equation (13). Because of the slow β-decay rates for the progenitor nuclei with $N = 82$, a long t_{FO} is required to decrease the progenitor abundance at $A = 129$. However, once the charge flow passes the bottleneck at $N = 82$, it reaches the progenitor nuclei at $A > 195$ relatively quickly. Consequently, the r-process nuclei at $A > 195$ are overproduced by about 40% in case H′ in order to satisfy the constraint on ^{129}I pro-

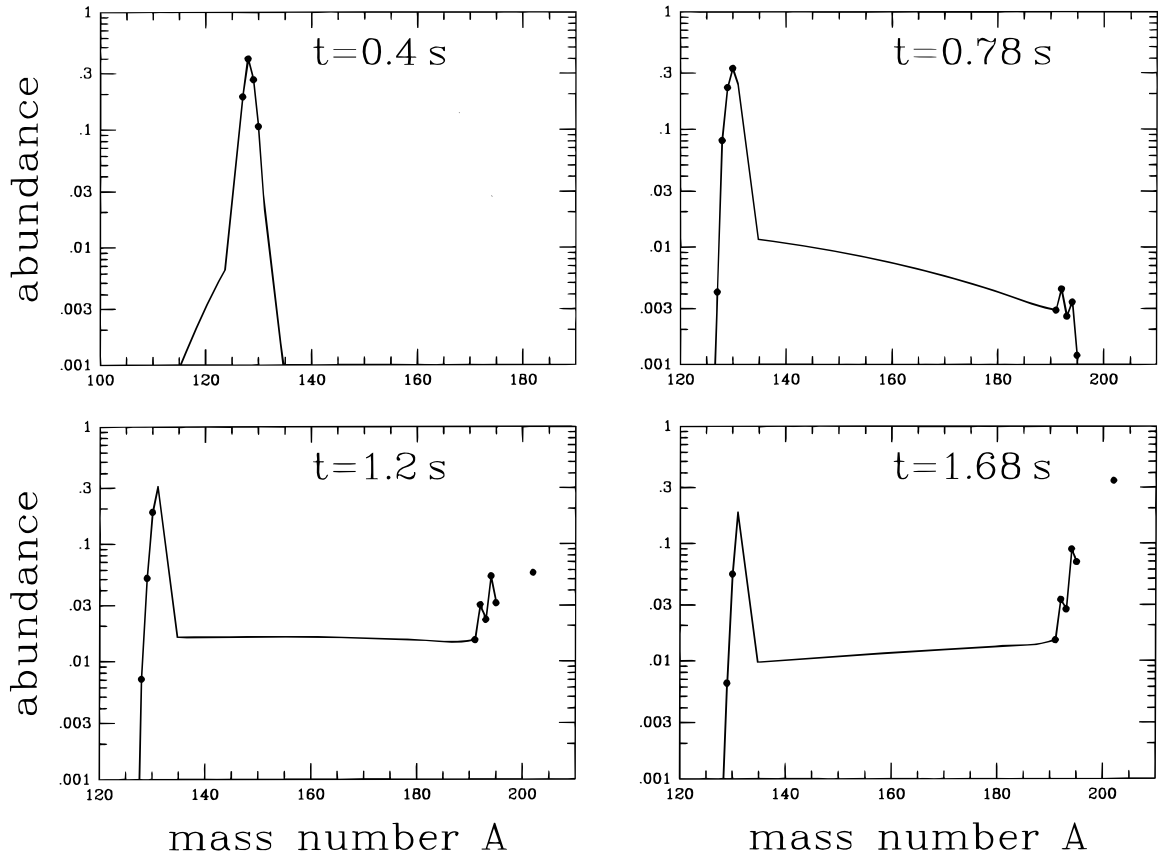

FIG. 7.—Same as Fig. 3, but for the case without neutrinos. Freezeout progenitor abundance patterns similar to those in cases H and L are obtained with neutron-to-seed ratios $n/s \approx 86$ and 44 at $t = t_{FO} \approx 1.68$ and 0.78 s, respectively.

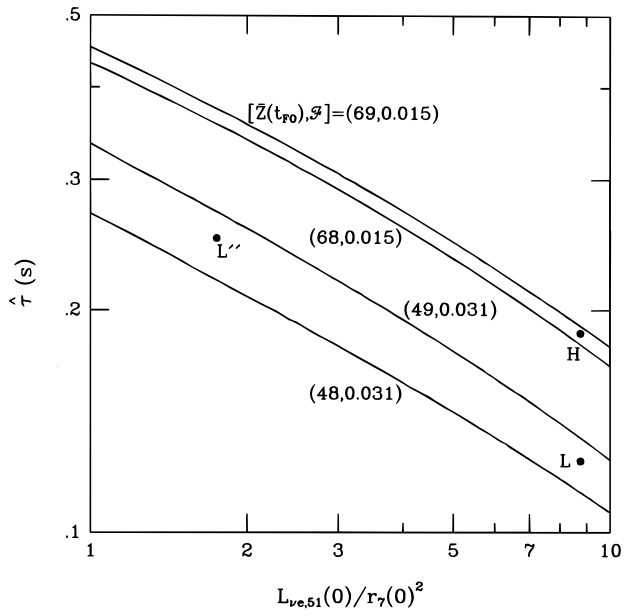

FIG. 8.—Parameter regions for $L_{\nu_e,51}(0)/r_7(0)^2$ and $\hat{\tau}$ in those cases similar to cases H and L. The solid lines correspond to the contours for the following values of the average progenitor charge at freezeout and the neutrino fluence after freezeout: $[\bar{Z}(t_{FO}), \mathcal{F}] = (48, 0.031)$, (49, 0.031), (68, 0.015), and (69, 0.015). For a neutron-to-seed ratio $n/s \sim 94$–96 (40–42), the parameters $L_{\nu_e,51}(0)/r_7(0)^2$ and $\hat{\tau}$ in those cases similar to case H (L) are most likely located in the region between the solid lines that includes the filled circle labelled H (L). For example, the combination of $L_{\nu_e,51}(0)/r_7(0)^2$ and $\hat{\tau}$ indicated as the filled circle labelled L″ is shown. This combination gives essentially the same freezeout progenitor abundance pattern as in case L, but with a lower $L_{\nu_e,51}(0)/r_7(0)^2$ and a longer $\hat{\tau}$. Consequently, we can choose generic cases H and L lying in the corresponding regions in this figure to give the same best fit to the gross solar r-process abundance pattern. All the constraints discussed in § 2.2 would be satisfied by these choices.

duction in equation (13). By comparison, the decaying ν_e flux in case H has the beneficial effect of accelerating the passage through the bottleneck at $N = 82$ at an earlier time without overproducing the r-process nuclei at $A > 195$ at later times. Furthermore, without neutrinos, the approximate β-flow equilibrium constraint in equation (14) is satisfied only for two progenitor nuclei ($Z = 47$–48) in the $N = 82$ peak in case L′. Therefore, while we cannot conclude that neutrinos are required to satisfy all the constraints derived from the observed solar r-process abundance data, the cases with neutrinos seem to be more attractive.

3.3. *Dependence on* $L_{\nu_e,51}(0)/r_7(0)^2$

We have presented the results for a fixed value of $L_{\nu_e,51}(0)/r_7(0)^2 \approx 8.77$ in § 3.1 and for the case without neutrinos corresponding to $L_{\nu_e,51}(0)/r_7(0)^2 = 0$ in § 3.2. We now examine the dependence of our results on $L_{\nu_e,51}(0)/r_7(0)^2$ while taking into account all the constraints discussed in § 2.2. In other words, we want to find those cases that are similar to case H or L but have different values of $L_{\nu_e,51}(0)/r_7(0)^2$.

As explained at the end of § 3.1, the solar r-process abundance ratios in equation (11) and the constraint on ^{129}I production in equation (13) require that the average progenitor charge at freezeout be $\bar{Z}(t_{FO}) = 68$–69 (48–49) in case H (L). Consequently, the neutron-to-seed ratio n/s in those cases similar to case H (L) has to be close to 94–96 (40–42). The other two parameters in our calculation, $L_{\nu_e,51}(0)/r_7(0)^2$ and $\hat{\tau}$, together with the freezeout time t_{FO}, are constrained by the average progenitor charge $\bar{Z}(t_{FO})$ at freezeout and the neutrino fluence $\mathcal{F}$ after freezeout (eq. [15] or [16]) in each case. Therefore, the combination of $L_{\nu_e,51}(0)/r_7(0)^2$ and $\hat{\tau}$ in those cases similar to case H would most likely be located in the region between the contour lines for $[\bar{Z}(t_{FO}), \mathcal{F}] = (68, 0.015)$ and (69, 0.015) on the $\hat{\tau}$ vs. $L_{\nu_e,51}(0)/r_7(0)^2$ plot. Likewise, the combination of $L_{\nu_e,51}(0)/r_7(0)^2$ and $\hat{\tau}$ in those cases similar to case L would most likely be located in the region between the contour lines for $[\bar{Z}(t_{FO}), \mathcal{F}] = (48, 0.031)$ and (49, 0.031) on the same plot. This plot is shown as Figure 8. Obviously, the parameter regions shown in Figure 8 include the best-fit parameters in cases H and L. We have checked a number of other combinations of $L_{\nu_e,51}(0)/r_7(0)^2$ and $\hat{\tau}$ within these regions and have confirmed that they give similar results to those discussed previously. In particular, the results corresponding to $L_{\nu_e,51}(0)/r_7(0)^2 \sim 1$ are very close to those in the case without neutrinos.

Furthermore, although the parameter $\hat{\tau}$ in case L is shorter than that in case H for the same $L_{\nu_e,51}(0)/r_7(0)^2$, we can find a case L″ that has a smaller $L_{\nu_e,51}(0)/r_7(0)^2$ and a longer $\hat{\tau}$ than both cases H and L (see Fig. 8) and, at the same time, gives a freezeout progenitor abundance pattern essentially identical to that in case L. Specifically, the parameters are $L_{\nu_e,51}(0)/r_7(0)^2 \approx 1.75$ [corresponding to $\lambda_{\nu_e}(Z, 0) \approx 10\ s^{-1}$ for the progenitor nuclei with $N = 82$], $\hat{\tau} \approx 0.25$ s, and $n/s \approx 47$ in case L″. The corresponding freezeout time is $t_{FO} \approx 0.66$ s. With the same weighting parameter $x \approx 2.17$ in equation (11), cases H and L″ give the same best fit to the gross solar r-process abundance pattern as cases H and L. It follows that a range of $L_{\nu_e,51}(0)/r_7(0)^2$ and $\hat{\tau}$ within the regions shown in Figure 8 can provide the yields in cases H and L.

4. CONCLUSIONS

We have found that the gross solar r-process abundance pattern near and above $A \sim 130$ can be reproduced by a superposition of two kinds of supernova r-process events after taking into account the meteoritic data on ^{129}I and ^{182}Hf. The first kind of events (case H) are mainly responsible for the r-process nuclei near and above $A \sim 195$. They also make a significant amount of the nuclei between $A \sim 130$ and 195, including ^{182}Hf, but very little ^{129}I. The r-process nuclei near $A \sim 130$ and the bulk of those between $A \sim 130$ and 195 are made in the second kind of events (case L). In each case, the r-process nucleosynthesis in a mass element expanding away from the protoneutron star is governed by the initial ν_e flux $L_{\nu_e,51}(0)/r_7(0)^2$ at the beginning of the r-process, the decay timescale $\hat{\tau}$ of the ν_e flux, and the neutron-to-seed ratio n/s. The parameter n/s specifies the r-process nuclei mainly produced in each case. The other two parameters, $L_{\nu_e,51}(0)/r_7(0)^2$ and $\hat{\tau}$, are important in determining when all the neutrons are used up, i.e., the freezeout time t_{FO}. Therefore, they determine the neutrino fluence $\mathcal{F}$ after freezeout, which may be responsible for the production of certain r-process nuclei through neutrino-induced neutron emission (Qian et al. 1997; Haxton et al. 1997). In addition, the ν_e flux plays a significant, possibly even crucial, role in decreasing the production of ^{129}I with respect to ^{182}Hf in case H. In both cases H and L, the solar r-process abundance ratios in equation (11) and the constraint on ^{129}I production in equation (13) determine the average progenitor charge

$\bar{Z}(t_{FO})$ at freezeout, and hence the neutron-to-seed ratio n/s. For a given $L_{\nu_e,51}(0)/r_7(0)^2$, the parameter $\hat{\tau}$, together with the freezeout time t_{FO}, can be calculated from $\bar{Z}(t_{FO})$ and the neutrino fluence constraint (eq. [15] or [16]) for each case, as shown in Figure 6. The dependence of $\hat{\tau}$ on $L_{\nu_e,51}(0)/r_7(0)^2$ is shown in Figure 8.

We wish to emphasize that the meteoritic constraint on coproduction of ^{129}I with ^{182}Hf leads to well-defined parameters, especially the neutron-to-seed ratio, in case H. As illustrated by the case without neutrinos, it is difficult to suppress the production of ^{129}I, which has an $N = 82$ progenitor nucleus with a long β-decay lifetime, and to avoid overproduction of the r-process nuclei at $A > 195$ at the same time. When ν_e capture is included in the r-process calculation, this difficulty is noticeably alleviated. However, the parameters characterizing the ν_e flux are then subject to additional constraints. Consequently, case H represents a particular kind of r-process events with possibly a very narrow range of neutron-to-seed ratios ($n/s \sim 90$). On the other hand, although we have shown that the gross solar r-process abundance pattern near and above $A \sim 130$ can be accounted for in the minimal scenario of two kinds of r-process events, the progenitor abundance pattern in case L can be regarded as some average over different events spanning a broader range of neutron-to-seed ratios (e.g., $n/s \sim 40$–50), as long as these events occur infrequently enough to be consistent with the meteoritic data on ^{129}I and ^{182}Hf. According to Wasserburg et al. (1996), the events in case H occur roughly once every 10^7 yr within a region of ~ 100 pc in size in the Galaxy, whereas those represented by case L occur roughly once every 10^8 yr in the same size region.

The size of ~ 100 pc may be understood from the expansion of the supernova ejecta. For an explosion energy of $\sim 10^{51}$ ergs, the initial velocity of the supernova ejecta is $v_0 \sim 10^3$ km s^{-1}. In about a few times 10^3 yr, the supernova sweeps over a distance of about 6 pc and mixes with about the same amount of the interstellar medium as the total mass M_{ej} of the original ejecta. At times $t \gg 10^3$ yr, the expansion (commonly known as "snow plowing") under momentum conservation is described by

$$R \approx \left(\frac{3}{\pi}\frac{M_{ej}\, v_0\, t_{exp}}{\rho_{ISM}}\right)^{1/4} \approx 63\left(\frac{t_{exp}}{10^7\ \mathrm{yr}}\right)^{1/4} \times \left(\frac{M_{ej}}{20\ M_\odot}\right)^{1/4}\left(\frac{v_0}{2\times 10^3\ \mathrm{km\ s^{-1}}}\right)^{1/4}\left(\frac{m_H\ \mathrm{cm^{-3}}}{\rho_{ISM}}\right)^{1/4} \mathrm{pc}\,, \quad (24)$$

where R is the radius of the expansion front from the center of the supernova, t_{exp} is the expansion time since the supernova explosion, ρ_{ISM} is the density of the interstellar medium, and m_H is the mass of the hydrogen atom. If we ignore other means of mixing such as Galactic rotation, clearly only those supernovae that could reach the position of the protosun within the lifetime of ^{182}Hf ($\tau_{182} \approx 1.3 \times 10^7$ yr) were responsible for the ^{182}Hf in the early solar system. From equation (24), those supernovae occurred within ~ 70 pc from the position of the protosun for reasonable values of the relevant parameters. Interestingly, within the lifetime of ^{182}Hf, the number of supernovae in a region of ~ 70 pc in size is about one, assuming a total Galactic volume of ~ 700 kpc^3 and a supernova frequency of $\sim (30\ \mathrm{yr})^{-1}$ in the whole Galaxy. Therefore, ^{182}Hf can be replenished on a timescale of $\sim 10^7$ yr consistent with the meteoritic data if the supernova r-process events in case H occur with a frequency of $f^H_{SN} \sim (30\ \mathrm{yr})^{-1}$ in the whole Galaxy, as also argued by Wasserburg et al. (1996).

On the other hand, the meteoritic data require that the ^{129}I produced along with ^{127}I be replenished on a much longer timescale of $\sim 10^8$ yr. Because the lifetimes of ^{129}I and ^{182}Hf are very close, the regions enclosing the supernovae contributing to these two nuclei have about the same size. Consequently, those supernova r-process events represented by case L must occur with a frequency of $f^L_{SN} \sim (300\ \mathrm{yr})^{-1}$ in the whole Galaxy. The frequencies f^H_{SN} and f^L_{SN}, together with the corresponding amounts of r-process ejecta M^H_r and M^L_r in cases H and L, determine the superposition parameter x in equation (11). As found in § 3, we have $x \sim (M^L_r/M^H_r)(f^L_{SN}/f^H_{SN}) \sim 1$–$2$. So the amount of r-process material ejected in the less frequent case L is ~ 10–20 times more than that in the more frequent case H. This implies that the mass loss rate is much higher, or more likely, that the period for ejecting r-process material is much longer in case L than in case H.

Following the preceding arguments for two distinct r-process sources, we propose the following r-process scenario assuming that all of the Type II supernovae producing r-process nuclei are of a generally similar nature. We suggest that material with higher neutron-to-seed ratios is ejected in the neutrino-driven winds at higher neutrino luminosities, i.e., at earlier times during the neutrino cooling phase of the protoneutron star. In addition, the early r-process ejecta have a neutron-to-seed ratio of $n/s \sim 90$. The neutron-to-seed ratio then rapidly decreases to ~ 40–50. If neutrino emission were uninterrupted, the neutron-to-seed ratio would stay at ~ 40–50, and the corresponding amount of material, all ejected, would be ~ 10–20 times more than the amount of material with $n/s \sim 90$. However, we consider that the continuous mass loss in the neutrino-driven winds is commonly terminated during the rapid transition from $n/s \sim 90$ to $n/s \sim 40$–50. This would occur in $\sim 90\%$ of the Type II supernovae, with only $\sim 10\%$ of them having prolonged continuous mass loss. Depending on, among other things, the initial core mass of the supernova progenitor, both neutrino emission and mass loss could be terminated by black hole formation during the neutrino cooling phase of the protoneutron star (Brown & Bethe 1994). In this scenario, there would then be $\sim 5 \times 10^8$ black holes with masses $\sim 1\ M_\odot$ from the r-process events in case H and $\sim 5 \times 10^7$ neutron stars from the less frequent r-process events represented by case L in the Galaxy today.

In the above r-process scenario, we have associated high neutron-to-seed ratios with high neutrino luminosities and low neutron-to-seed ratios with low neutrino luminosities. Qualitatively, a shorter $\hat{\tau}$ is expected for a higher neutrino luminosity (Qian & Woosley 1996). This can be achieved in the framework of the present model (see cases H and L″ in Fig. 8). Of course, a consistent set of the three parameters $L_{\nu_e,51}(0)/r_7(0)^2$, $\hat{\tau}$, and n/s at different times during the neutrino cooling phase of the protoneutron star can only be obtained in a detailed numerical study of Type II supernovae.

We note that many other nuclear species are produced by the explosive nucleosynthesis (e.g., Fe and Si) in Type II supernovae and by the hydrostatic burning (e.g., ^{16}O) in the

outer envelope during the presupernova evolution. The explosive nucleosynthesis is associated with the shock propagation through the envelope. The products from both the explosive nucleosynthesis and the hydrostatic burning are largely unaffected by the neutrinos from the protoneutron star (except for the ν-process discussed by Woosley et al. 1990) or by the possible formation of a black hole during the neutrino cooling phase of the protoneutron star. Therefore, the abundant non–r-process nuclei are ejected together with the r-process elements in a Type II supernova. The scenario given here would not significantly alter the usual supernova contributions to the non–r-process nuclei.

Furthermore, we note that neutrino-driven winds also develop after the accretion-induced collapse (AIC) of a white dwarf into a neutron star (Woosley & Baron 1992). Therefore, the AIC events could also correspond to the infrequent r-process events represented by case L. However, because there is no envelope around the final neutron star in the AIC events, the overall nucleosynthetic signature of such events is different from that of Type II supernovae. Only the nuclear species produced in the neutrino-driven winds, especially the r-process nuclei, are ejected in the AIC events.

Finally, the diversity of r-process sources have some interesting consequences for Galactic chemical evolution. At very low metallicities, only Type II supernovae could make Fe, whereas both Type Ia and Type II supernovae contribute to Fe at sufficiently high metallicities. Therefore, if the r-process events in case H were mainly associated with Type II supernovae, the abundance ratio of the corresponding main r-process product with respect to Fe would remain constant at low metallicities and decrease with increasing metallicity after Type Ia supernovae began to make Fe. On the other hand, if the r-process events represented by case L were mainly associated with the AIC events, the metallicity dependence for the abundance ratio of the corresponding main r-process product with respect to Fe would be sensitive to the difference between the time at which such events first occurred and the onset of increase in metallicity caused by Type Ia supernova.

The above suggestions regarding the nature of supernova r-process events are highly speculative. However, if the binary distribution of r-process sources with very different frequencies and very different mass contributions is correct, then some new supernova r-process models along the general lines indicated here will be required.

We want to thank Gerry Brown and Sterl Phinney for valuable discussions. We also want to thank the referee, Al Cameron, for helpful comments. This work was supported in part by the US Department of Energy under Grant No. DE-FG03-88ER-40397, by NASA under Grant No. NAG 5-4076, and by Division Contribution No. 5827(973). Y.-Z. Qian was supported by the David W. Morrisroe Fellowship at Caltech.

REFERENCES

Brown, G. E., & Bethe, H. A. 1994, ApJ, 423, 659
Burbidge, E. M., Burbidge, G. R., Fowler, W. A., & Hoyle, F. 1957, Rev. Mod. Phys., 29, 547
Cameron, A. G. W. 1957, PASP, 69, 201
Cameron, A. G. W., Cowan, J. J., Klapdor, H. V., Metzinger, J., Oda, T., & Truran, J. W. 1983, Ap&SS, 91, 221
Fuller, G. M., & Meyer, B. S. 1995, ApJ, 389, 517
Goriely, S., & Arnould, M. 1996, A&A, 312, 327
Haxton, W. C., Langanke, K., Qian, Y.-Z., & Vogel, P. 1997, Phys. Rev. Lett., 78, 2694
Hoffman, R. D., Woosley, S. E., & Qian, Y.-Z. 1997, ApJ, 482, 951
Käppeler, F., Beer, H., & Wisshak, K. 1989, Rep. Prog. Phys., 52, 945
Kratz, K.-L., Bitouzet, J.-P., Thielemann, F.-K., Möller, P., & Pfeiffer, B. 1993, ApJ, 403, 216
Kratz, K.-L., Thielemann, F.-K., Hillebrandt, W., Möller, P., Harms, V., Wöhr, A., & Truran, J. W. 1988, J. Phys. G, 14, S331
Mathews, G. J., Bazan, G., & Cowan, J. J. 1992, ApJ, 391, 719
McLaughlin, G. C., & Fuller, G. M. 1996, ApJ, 464, L143
———. 1997, ApJ, 489, 766
Meyer, B. S. 1995, ApJ, 449, L55
Meyer, B. S., Howard, W. M., Mathews, G. J., Woosley, S. E., & Hoffman, R. D. 1992, ApJ, 399, 656
Möller, P., Nix, J. R., & Kratz, K.-L. 1997, At. Data Nucl. Data Tables, 166, 131
Qian, Y.-Z., Haxton, W. C., Langanke, K., & Vogel, P. 1997, Phys. Rev. C, 55, 1532
Qian, Y.-Z., & Woosley, S. E. 1996, ApJ, 471, 331
Sneden, C., McWilliam, A., Preston, G. W., Cowan, J. J., Burris, D. L., & Armosky, B. J. 1996, ApJ, 467, 819
Takahashi, K., Witti, J., & Janka, H.-Th. 1994, A&A, 286, 857
Wasserburg, G. J., Busso, M., & Gallino, R. 1996, ApJ, 466, L109
Witti, J., Janka, H.-Th., & Takahashi, K. 1994, A&A, 286, 841
Woosley, S. E., & Baron, E. 1992, ApJ, 391, 228
Woosley, S. E., Hartmann, D. H., Hoffman, R. D., & Haxton, W. C. 1990, ApJ, 356, 272
Woosley, S. E., & Hoffman, R. D. 1992, ApJ, 395, 202
Woosley, S. E., Wilson, J. R., Mathews, G. J., Hoffman, R. D., & Meyer, B. S. 1994, ApJ, 433, 229